Universiteit Antwerpen

This item is the archived peer-reviewed author-version of:

Influence of flow and pressure distribution inside a gas diffusion electrode on the performance of a flow-by CO2 electrolyzer

Reference:
De Mot Bert, Hereijgers Jonas, Duarte Miguel, Breugelmans Tom.- Influence of flow and pressure distribution inside a gas diffusion electrode on the performance of a flow-by CO2 electrolyzer
Chemical engineering journal - ISSN 1385-8947 - 378(2019), UNSP 122224
Full text (Publisher's DOI): https://doi.org/10.1016/J.CEJ.2019.122224
To cite this reference: https://hdl.handle.net/10067/1617100151162165141

uantwerpen.be
Institutional repository IRUA

Influence of flow and pressure distribution inside a gas diffusion electrode on the performance of a flow-by CO2 electrolyzer

Bert De Mot[1], Jonas Hereijgers[1], Miguel Duarte[1], Tom Breugelmans[1, 2, *]

[1] *Research group Applied Electrochemistry & Catalysis, University of Antwerp, Universiteitsplein 1, 2610 Wilrijk, Belgium*
[2] *Separation & Conversion Technologies, VITO, Boeretang 200, 2400 Mol, Belgium.*

*Corresponding author: tel. (+) 32/ 3.265.2370; e-mail: tom.breugelmans@uantwerpen.be

Abstract

Over the last few years, the scientific community has paid lots of interest in the electrochemical CO_2 reduction (ECR) as a possible solution for earth's global warming and the transitioning to a CO_2 neutral industry. The majority of the researchers focus on improving the catalyst material, leading to higher current densities at lower cell potentials and increased selectivities. However, so far, little attention has been given to the investigation and optimization of the ECR reactor design and process parameters, which are equally, if not more, important in order to up-scale the process towards an industrial level. In this work the ECR towards formate on tin nanoparticles in a flow-by electrolyzer is discussed. Special attention is given to the lay-out of both the reactor and the overall process. Additionally, the influence of the differential pressure across the gas diffusion electrode (GDE) on the reactor performance is investigated. It was found that by controlling the differential pressure, the perspiration, or leaking of electrolyte through the GDE, could be controlled and minimized. Results show that by controlling the differential pressure at 0 mbar, perspiration is minimal and that an optimal CO_2 diffusion can be achieved, leading to an overall FE of 76% over 6 hours at 100 mA/cm². Furthermore, due to the electro-wetting effect of the GDE, it was impossible to operate the reactor without perspiration, thereby avoiding the risk of salt crystallization in the reactor. Overall this study strengthens the idea that flow-by electrolyzers are promising reactors for the industrialization of electrochemical CO_2 conversion and that pressure regulation is essential to obtain optimal process conditions.

Keywords

CO_2 reduction; electrochemistry; electrochemical engineering; electrosynthesis; formate

1. Introduction

Since the start of the industrial revolution the concentration of CO_2 in the atmosphere has increased drastically leading to a concentration above 400 ppm [1,2]. Nevertheless, it is essential to decrease future CO_2 emissions in the atmosphere if we want to reduce the negative impact of global warming. As a result, many researchers have turned their attention towards the investigation of Carbon Capture and Storage (CCS) and Carbon Capture and Utilization (CCU) technologies, leading to a wide range of improved techniques such as CO_2 absorption, membrane separators, photo reduction and electrochemical reduction [3].

Due to the combined positive effects of CCS and electrochemistry, the study of electrochemical CO_2 reduction (ECR) has received a lot of attention from the scientific community during the past decade [4–10]. Up to now, the research field primarily focused on the optimization of the cathode material, trying to improve the product selectivity, overpotential and stability of the process. As a result significant progress has been made in the field of electrocatalyst development. For example by using copper electrodes the faradaic efficiency (FE) towards ethanol, methane and ethylene reached values up to 38%, 50 and even 70% respectively [11–13]. By using nanostructured silver electro catalyst instead of copper, carbon monoxide could be produced with a FE of 94% [14]. Another interesting product of ECR is formate, which has four major advantages: (i) cheap earth abundant metal catalysts such as tin and lead can be used to yield high selectivities [9,15], (ii) the liquid state of the product enables easy and cheap storage, (iii) the reaction mechanism of CO_2 to formate is a two electron mechanism, this simple mechanism reduces the likelihood of byproducts and (iv) as a feedstock for the chemical industry, formate already has a wide variety of industrial applications [16].

While the understanding of the molecular details at the catalyst surface is ever more growing, resulting in highly active and selective electrocatalysts, so far little attention has been given to the optimization of the reactor design, which is equally, if not, more important to obtain an

economically viable process [17–19]. This is demonstrated clearly in the literature survey executed by Endrõdi et al., which shows that out of 400 ECR papers written in 2016 only 10 authors used a continuous flow set-up [20]. From these limited results it is clear that improved reactor and system design leads to higher current densities and higher product yields due to better mass transport in the cell [21], lower ohmic resistance and lower cell potential [22]. Although improvements in reactor design have been made, additional research on reactor design is needed in order to upscale the process towards economically feasible electrolyzers for industry [19,23,24].

An important aspect in electrochemical reactor engineering for the ECR is mass transfer of CO_2 towards the cathode surface. Recent studies show that the mass transfer limitations due to low CO_2 solubility can be reduced by using a gas diffusion electrode (GDE) combined with gaseous CO_2 [18,25]. Jeanty et al. demonstrated this type of reactor lay-out containing silver as electrocatalyst when upscaling an electrolyzer for the ECR towards CO [26]. Operating in flow-by mode, the CO_2 gas flows over the surface of the GDE and by diffusion enters the GDE in the direction of the catalyst surface. At the same time the catholyte flows at the opposite side along the GDE. The major advantages of using flow-by mode is the ability for stable and long-term operation as described by Jeanty et al. [26]. Additionally, since the gas is not pressed through the GDE, no gas bubbles are present in the catholyte flow channel which has a positive impact on the overall cell resistance and the energy efficiency of the reactor. Using this flow-by mode, Jeanty et al. described leaking of the catholyte towards the gas channel through the GDE. This phenomenon, also called perspiration, is due to the combined effects of electro-wetting of the GDE and the difference in pressure between the catholyte side and the gas side of the GDE, also called ‘differential pressure’, given by Eq 1., with P being the pressure.

$$\Delta P_{\text{differential}} = P_{\text{catholyte}} - P_{\text{gas}} \qquad \text{Eq. 1}$$

The goal of perspiration is to prevent salts from crystalizing into the pores, blocking otherwise the CO_2 from reaching the catalyst surface and consequently decreasing productivity and selectivity. However, perspiration itself can also block the pores and subsequently preventing CO_2 from entering the GDE which could lead to a lower reactor performance. Hence, the differential pressure across the GDE is important to control the level of perspiration and consequently the mass transfer rate of CO_2. Although this effect was already briefly mentioned by Jeanty et al., no thorough research on the underlying mechanism and optimization has been conducted [26]. In this work, for the first time, the underlying mechanism of perspiration and its influence on the reactor performance as function of the differential pressure was studied and discussed for the ECR to formate on tin nanoparticles.

2. Materials and methods

2.1 Chemicals

Tin nanopowder (< 150nm, >99%) and Nafion perfluorinated resin solution (5 wt%) was purchased from Sigma-Aldrich (Belgium). Potassium carbonate (extra pure) and isopropyl alcohol (99.8%, electronic use) were purchased from Acros Organics (Belgium) and potassium hydroxide was purchased from VWR (Belgium). Ultrapure water was prepared in the laboratory (Milli-Q gradient, Millipore, USA). The Nafion 117 membrane, platinized titanium screen (SKU: 592777) and Sigracet 39 BC GDL were purchased from Fuel Cell store (USA). CO_2 (99.998 %), N_2 (99.999 %), Ar (99.999 %) and He (99.999 %) were purchased from Nippon (Belgium).

2.2 GDE preparation

To deposit the catalyst onto the GDE, a catalyst ink was prepared. Tin nanopowder was mixed with the Nafion perfluorinated resin with a mass ratio of respectively 70/30. Next, this mixture was diluted in isopropyl alcohol resulting in a concentration of 3 wt% solids. To

disperse the nanoparticles and create a homogenous mixture, the ink was sonicated (VWR, USC 300TH) for 30 minutes. After sonication, the ink was airbrushed (Conrad Electronic, AB-200) on the microporous layer (MPL) of the Sigracet carbon paper cut to size with a geometrical surface area of 16 cm² at an ambient temperature of 60°C to promote the drying of the ink. Argon was used as carrier gas. The carbon paper was dried for 30 minutes and weighted before and after the deposition of the ink to ensure a correct catalyst loading of 0.75 mg/cm². Del Castillo et al. demonstrated an optimal reduction of CO_2 towards formic acid on tin nanoparticles with a catalyst load of 0.75 mg/cm² and a particle size of 150 nm [27]. SEM (Quanta 250 FEG, potential 5kV, spot size 3.5) was used to check the distribution of Sn nanoparticles, see supporting information. All GDEs used in the experiments had a catalyst loading of 0.75 +/-0.05 mg/cm² and the catalyst particles were evenly distributed. After the electrochemical experiments the catholyte was analyzed using ICP-MS (Agilent 7500) to determine the concentration of detached Sn particles. A standard of Sn was used (Alfa Aesar, Ward Hill, USA) in the same range as the sample, all samples and standards were diluted with 1% HCl (Fluka TraceSelect, Morris Planes, USA).

2.2 Electrochemical reactor design

The continuous flow-by ECR experiments were performed in a custom designed reactor (Euromod MP 45, Imes), the detailed layout of this reactor is presented in figure 1. The CO_2 entered the reactor at the top. Convective gas flow through the GDE was prevented at all times by keeping the pressure at the gas side lower than at the liquid side of the GDE. A Nylon mesh was placed inside the gas flow channel to act as a turbulence promotor. The GDE itself separated the catholyte from the gas compartment with the tin coated side of the GDE faced towards the catholyte. Both the unreacted CO_2 and the perspirated catholyte left the reactor at the bottom through the CO_2 outlet. The GDE acted as cathode and was connected to

the potentiostat (Metrohm, Multi Autolab M204, 10A booster module) using a titanium current collector. As anode a platinized titanium screen (Fuel Cell store, USA) was used and similar to the cathode a titanium current collector was used to ensure an electrical connection with the potentiostat.

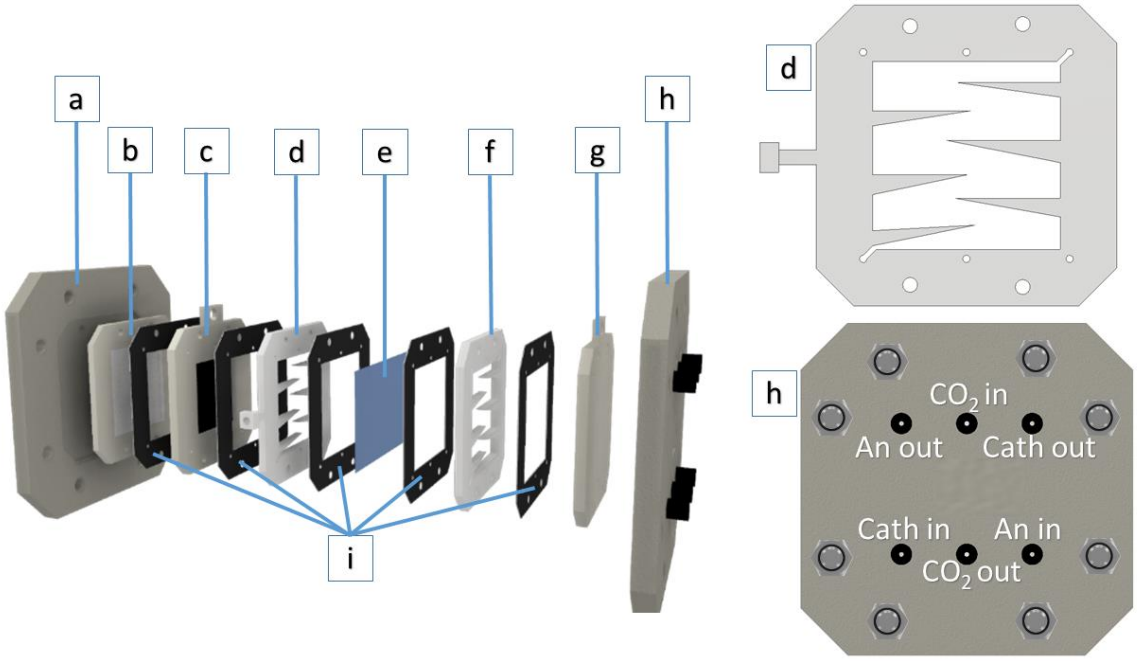

Figure 1. Graphical representation of the flow-by reactor: aluminum back-plate (a); gas flow channel (b); cathode: GDE (16cm²) + titanium current collector(c); catholyte flow channel (d); Nafion membrane (e); anolyte flow channel (f); anode: platinized screen + titanium current collector (g); aluminum front-plate with 6mm push-in connections (h); 1 mm thick Viton gaskets (i).

Both the catholyte and the anolyte entered the reactor at separate inlets which were placed at the bottom of the reactor. PMMA spacers (Figure 1d and 1f) were used for the fluid control of the electrolyte and had "tooth shaped" structures that served a dual purpose: (i) they resulted in a serpentine channel which helped to increase the mass transfer towards the catalyst surface and the removal of the products and (ii) they provided mechanical support for the GDE and the Nafion membrane. In the catholyte flow channel a 1 mm leak free Ag/AgCl reference electrode (Innovative Instruments Inc.) was inserted.

To separate the catholyte from the anolyte compartment, to prevent product crossover and to enable ion transport, a Nafion 117 membrane was used which was pressed between the electrolyte flow channels. All the fluid connections (Lefort, 33000605N) were located at the front-plate of the reactor and fluid distribution was ensured through an internal manifold. Finally 1 mm thick Viton (Eriks) gaskets were used to ensure a leak free operation. The reactor was mechanically sealed using M6 bolts at 4 Nm.

A schematic overview of the complete system is shown in figure 2. Mass flow controllers (Brooks instruments, GF 040) were used to accurately supply a constant flow of CO_2 to the system, the accuracy of the mass flow controllers is +/- 2 ml/min. Before entering the reactor, the CO_2 was humidified by purging at room temperature. As catholyte, 0.5 M $KHCO_3$ and as anolyte 2 M KOH were selected since these solutions have shown great performance towards CO_2 reduction and oxygen evolution respectively [17,28,29]. The catholyte and anolyte were stored separately in storage tanks. Both storage tanks had a volume of 1000 ml and were filled with 500 ml electrolyte. Inside the reactor, K^+ ions will move through the Nafion membrane due to migration caused by the applied potential. Over time this will cause a depletion of K^+ ions in the anolyte which results in a decrease of conductivity and an increase in cell resistance. To avoid this problem each experiment was started with fresh electrolyte. A multi-channel peristaltic pump (Ismatec, Reglo ICC) was used to recirculate the electrolyte through the reactor at a constant flow rate of 20 ml/min. After flowing through the reactor, the catholyte was combined with the outlet stream of the gas channel. In the catholyte storage tank the unreacted CO_2 was purged through the catholyte, afterwards the gas mixture was separated from the electrolyte flow and the gas was analyzed using a GC-TCD (Shimadzu 2014, Japan) in combination with a Shin carbon St 100/120 2mx1mm column (Restek, USA). 10 ml/min helium was used as carrier gas. The column temperature was held constant at 40°C

for 3 minutes, afterwards the temperature increased 40°C/min to 250°C. A HPLC (Alliance 2695, Waters, USA) combined with a packed column (IC-Pak, Waters, USA) and a PDA detector (2996, Waters, at 210 nm) was employed to detect the formate concentration in the catholyte. A perchloric acid solution (0.1%) was used as the eluant for the HPLC. The error on the presented FE data is lower than 2.7%. The potentiostat was used to supply a constant current of 100 mA/cm² to the cell.

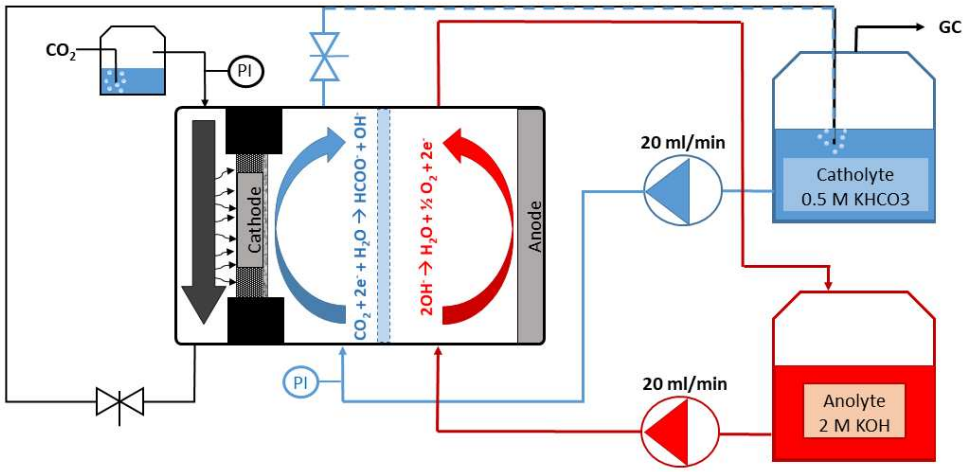

Figure 2. Schematic overview of the complete system: anolyte flow (red), catholyte flow (blue) and gas flow (black).

As mentioned in the introduction, the goal was to study the influence of the perspiration on the reactor performance by controlling the differential pressure. This was achieved by implementing two needle valves (Lefort, 2175-1152): one in the outlet of the catholyte flow channel and one in the outlet of the gas flow channel. These valves were used to control the backpressure inside the reactor. The pressure inside the reactor compartments were measured using two sensors (Gefran, TK-series) with an accuracy of +/- 2.5 mbar, which were installed on the inlet of the gas channel and the catholyte flow channel. The pressure was logged during the experiment (National Instruments, USB 6000).

3. Results and discussion

3.1 Influence of the perspiration flow rate on the reactor performance.

To study the influence of the perspiration, the CO_2 flow rate was fixed at 50 ml/min to exclude any effects from the diffusion boundary layer at the GDE, see supporting information. Each experiment lasted 6 hours and every hour a sample was taken and analyzed from the gas outlet and catholyte and this as function of the differential pressure over the GDE. Figure 3 shows the progress of the FE over 6 hours. A constant differential pressure of 18.5 mbar was maintained during the experiment, perspiration is present at this intermediate differential pressure, but not to excessive. From these results, it can be seen that after one hour the FE of formate equals 76%. In the subsequent hours the FE of formate however dropped drastically to 26% after six hours. Formate accumulated in the recycling catholyte and consequently due to the decrease in FE, the average FE of formate over the entire length of the experiment was only 46%. This decrease of FE was compensated by an increasing FE of H_2 over the length of the experiment, leading to an average FE of 45%. The FE for CO remained constant at 6%. One of the main reasons for this is linked to a substantial decrease of the pH, which will be further explained in section 3.2.

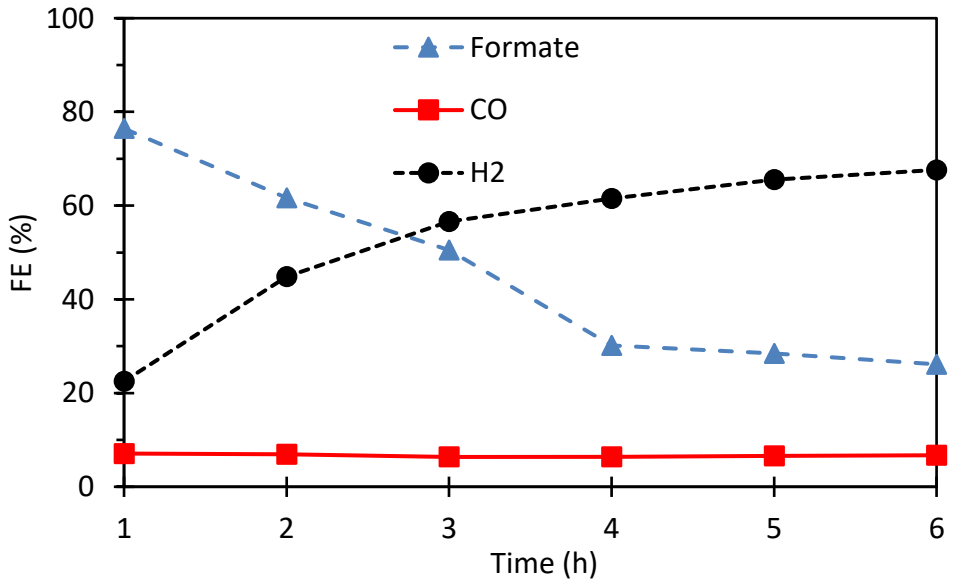

Figure 3. Average FE plotted as function of time (h) at a constant current of 100 mA/cm², constant differential pressure of 18.5 mbar and a CO_2 flow rate of 50 ml/min: Formate (blue, triangle); CO (red square); H_2 (black, circle)

The influence of the differential pressure on the average FE after 6 hours of formate, CO and H_2 is represented in Figure 4. From these results it can be observed that formate is the major product. However, no significant decrease in formate FE can be observed from the plot. Even at 80 mbar, when the perspiration flow rate was 18 ml/min,, still a FE of 61% towards formate was measured. This is in contrast with the assumption that an increase in differential pressure and perspiration leads to flooding of GDE pores and reduces the CO_2 diffusion substantially [26]. This unexpected result is caused by two major parameters: First, the effect of saturation of electrolyte with unreacted CO_2. Second, the influence of the morphology of the GDE. Both parameters are discusses in the sections, 3.2 and 3.3 respectively. Furthermore it was observed that the reactor was not in flow-by mode at negative differential pressures, hence only positive differential pressures are presented in Fig. 5.

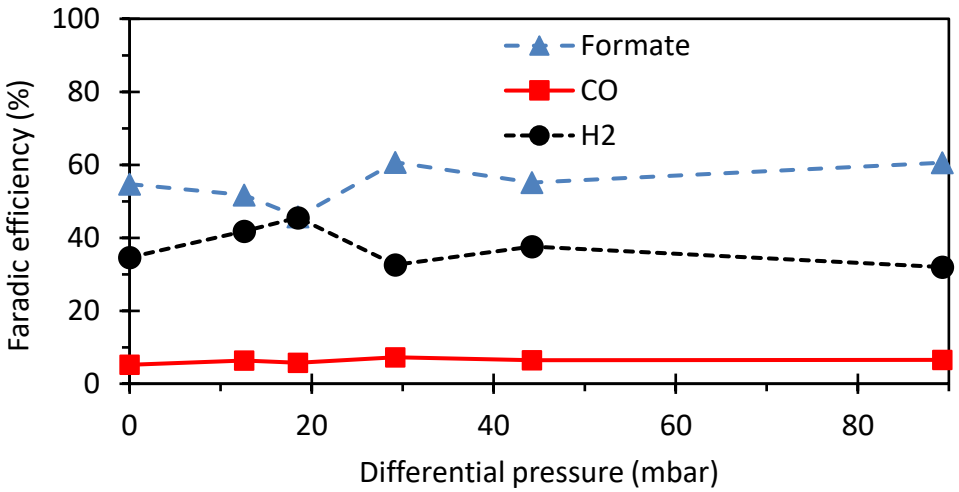

Figure 4. FE plotted as function of differential pressure at a constant current of 100 mA/cm², CO_2 flow rate of 50 ml/min, runtime = 6 hours: Formate (blue, triangle); CO (red square); H_2 (black, circle)

3.2 Effect of electrolyte saturation

As described in the previous section it was seen that flooding of the GDE did not lead to a decrease of the FE towards formate as was initially predicted. This result is due to two major parameters, one of them is the saturation of electrolyte with unreacted CO_2. Dissolved CO_2 compensates for the reduced diffusion rate of gaseous CO_2, in addition it lowers the pH of the electrolyte which has a negative effect on the CO_2 electro reduction. To this end, the catholyte storage tank was adjusted, such that CO_2 was no longer purged into the catholyte (Fig. 5). In the adjusted set-up (b) the gas outlet stream entered the catholyte storage tank separately and was no longer purged through the electrolyte. The storage tank allowed the perspirated catholyte to be separated from the gas flow and at the same time CO_2 was prevented from purging in the electrolyte, minimizing its dissolution. Consequently, the main source of CO_2 now had to come from the gas flow and the negative effects of perspiration onto the CO_2 mass transfer were no longer masked by the dissolved CO_2.

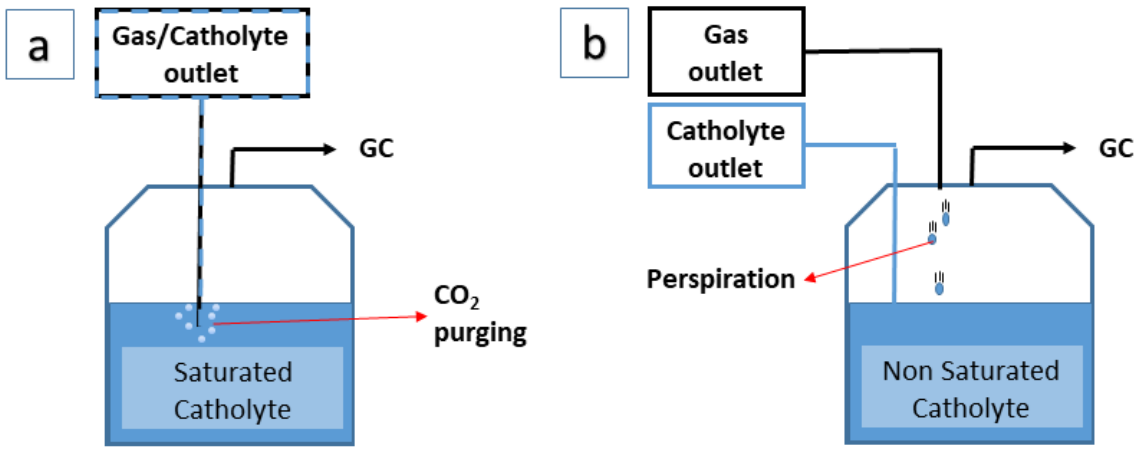

Figure 5: Adjustment of the catholyte storage tank set-up to prevent saturation of the electrolyte: original set-up (a) and adjusted set-up (b)

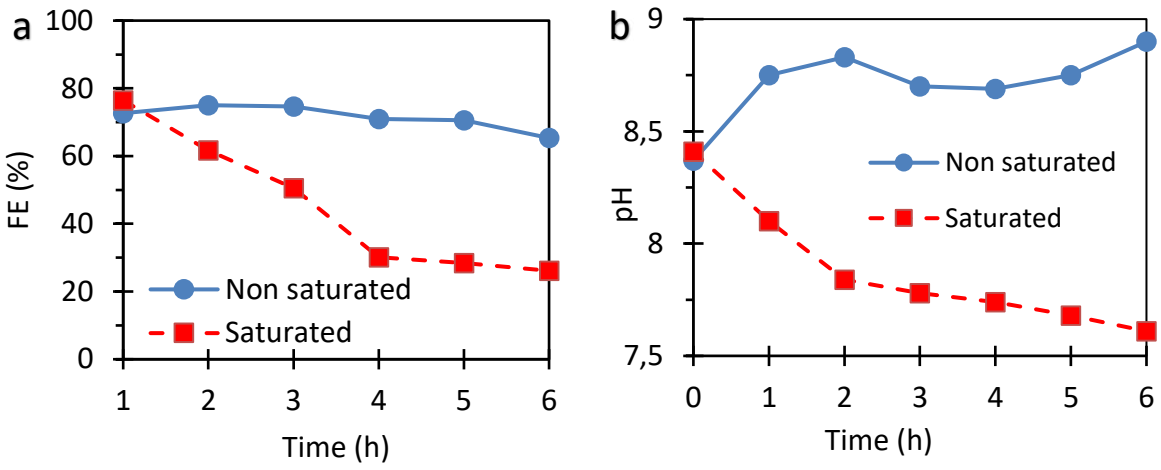

Figure 6: FE of formate (a) and pH (b) as function of the run time at a catholyte flow rate of 20 ml/min, a CO_2 flow rate of 50 ml/min, a differential pressure of 18.5 mbar ± 0.5 mbar and a constant current of 100 mA/cm². Samples of the accumulating formate were taken every hour. Catholyte: 0.5 M $KHCO_3$ non-saturated (blue, circle) ; 0.5M $KHCO_3$ saturated with CO_2 (red, square). Anolyte: 2M KOH.

Doing so, the FE for both saturated and non-saturated electrolyte with CO_2 after one hour were almost identical, 76% and 72% respectively (Figure 6). As the experiment proceeded, a decrease in FE was observed when saturated electrolyte was used, as was already observed in the previous section (§3.1). However when the non-saturated electrolyte was used, the decrease of FE was lower and limited to 7%. After 6 hours the FE was 65% and the average FE over the entire experiment was 72%, this limited decrease was mainly caused by the coalescence and to a smaller extend to the detachment of Sn nanoparticles as shown in the supporting information.

The decrease of FE observed when saturated electrolyte was used was a result of the change in pH caused by the formation of carbonic acid, as shown in Eq. 2.

$$CO_2(aq) + H_2O\,(aq) \leftrightarrow H_2CO_3(aq) \leftrightarrow H^+(aq) + HCO_3^-(aq) \qquad \text{Eq.2}$$

Formed carbonic acid will, on its turn, dissociate resulting in the release of a proton into the catholyte solution. By continuous saturation of the electrolyte the equilibria reaction is pushed towards the right side of the equilibrium, leading to an increase in proton concentration. This decrease of pH favors the evolution of hydrogen gas and hinders the production of formate. To evaluate this phenomena, the pH of both the non-saturated and saturated electrolyte was measured during 6 hours of electrolysis and are presented in Figure 6 (b). The figure shows the decrease of pH due to the reaction of CO_2. After 6 hours the pH of the non-saturated electrolyte was 8.90 while the pH of the saturated electrolyte dropped to 7.61, causing the FE of formate to drop. After 6 hours the pH is not stable and is slightly decreasing. This is due to the fact that an equilibrium is in play between the acidification of the electrolyte due to the saturation of CO2 and the alkalization of the electrolyte caused by the formation of hydroxide ions at the cathode surface.

In addition, the concentration of formate is presented in Figure 7 for both the saturated and unsaturated experiment. Due to the recirculation of catholyte, the formate is accumulated in the solution. After the first hour the concentration is 2 g/l for both the saturated and the unsaturated experiment. Afterwards the concentrations drifted apart, this is due to the major decrease of FE when saturated electrolyte was used. The final concentration of formate was 11.05 g/l and 7.04 g/l for the non-saturated and the saturated experiment respectively. Furthermore the cathode potential during the experiment was -2.98 V vs Ag/AgCl for the non-saturated experiment and 2.82 V vs Ag/AgCl for the saturated experiment. This small difference in cathode potentials is due to the lower conductivity of non-saturated electrolyte compared to saturated electrolyte.

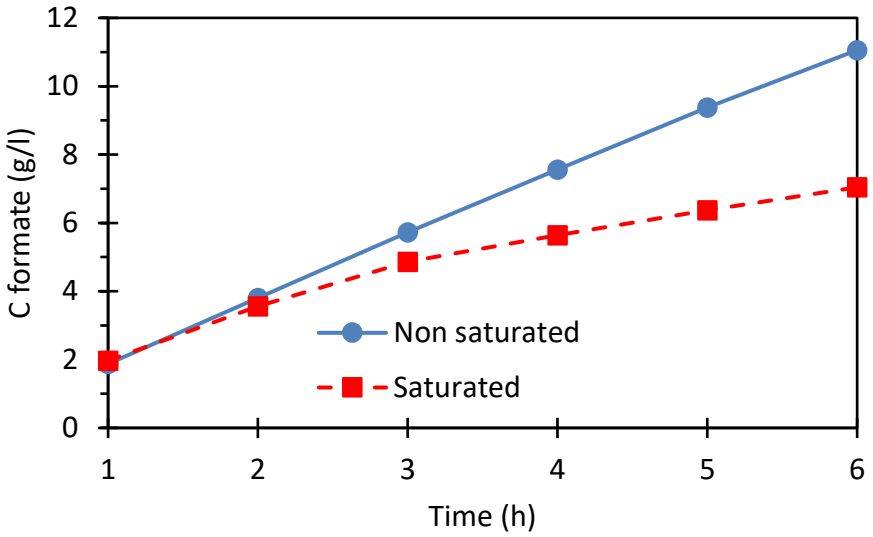

Figure 7: Concentration of formate as function of the run time at a catholyte flow rate of 20 ml/min, a CO_2 flow rate of 50 ml/min, a differential pressure of 18.5 mbar ± 0.5 mbar and a constant current of 100 mA/cm². Samples of the accumulating formate were taken every hour. Catholyte: 0.5 M $KHCO_3$ non-saturated (blue, circle) ; 0.5M $KHCO_3$ saturated with CO_2 (red, square). Anolyte: 2M KOH.

The ECR experiment was repeated for a range of differential pressures using the non-saturated electrolyte. The average FE for formate is represented as function of differential pressure in Figure 8 for both conditions (i.e. saturated and non-saturated electrolyte).

A 20% FE difference between saturated and non-saturated electrolyte at 0 mbar differential pressure was observed, which can most likely be explained by the pH change of the electrolyte due to the formation of bicarbonate leading to favored hydrogen evolution. In addition, the graph for the non-saturated electrolyte reveals that the FE reached a peak value of 76% at 0 mbar differential pressure and slightly decreased with increasing differential pressure upto 70% FE at 80 mbar, showing the effect of perspiration. However since a high increase in the perspiration flow rate was observered at 80 mbar compared to 0 mbar, it was expected that the influence on the FE would be much larger. This limited influence of perspiration flow rate on the FE of formate is a result of the morphology of the GDE which is described in section 3.3.

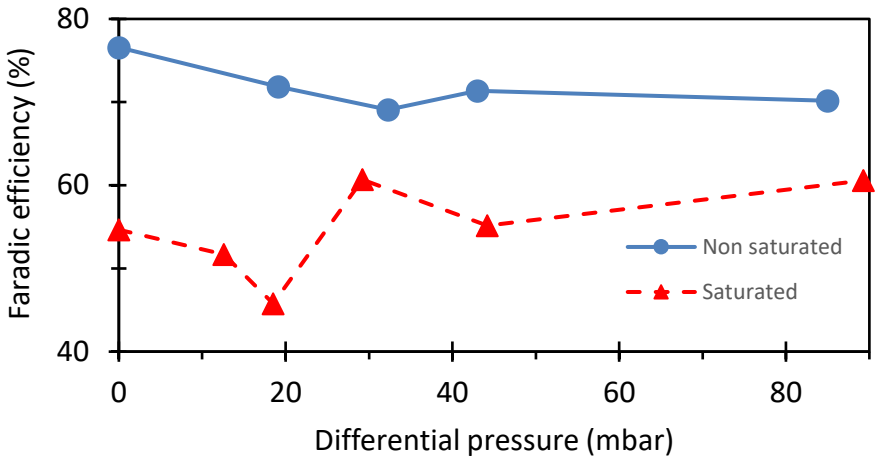

Figure 8: Average FE for formate as function of differential pressure at a catholyte flow rate of 20 ml/min, a CO_2 flow rate of 50 ml/min and a constant current of 100 mA/cm², run time = 6 hours. Catholyte: 0.5 M $KHCO_3$ non-saturated (blue, circle) ; 0.5M $KHCO_3$ saturated with CO_2 (red, triangle). Anolyte: 2M KOH.

3.3 Assessment of perspiration during electrolysis

To understand the limited influence of the perspiration flow rate on the FE, as seen in Figure 8 (non-saturated), it is essential to gain thorough insight in the underlying mechanism of the perspiration process or how it affects the reactor performance. Perspiration can be attributed to two effects: (i) the electro-wetting effect, attributed to the change in hydrophobic character of the GDE when current is applied and (ii) the differential pressure across the GDE. To investigate these effects, the perspiration flow rate was measured over a range of differential pressures and the flooding of the GDE was visually monitored. To this end, the aluminum back plate was replaced with a transparent PMMA plate, allowing to observe the perspiration. The different stages of the perspiration process are presented in Figure 9, for the clarity of the reader the four stages (a-d) are explained in the following paragraph. (a) Before current was applied, the GDE was dry and no perspiration was observed. (b) As soon as current (100 mA/cm²) was applied, small perspiration droplets started to emerge on the GDE. The

perspiration is influenced by the electro-wetting effect of the GDE as it only appears after the current was applied. (c) Over time the droplets increased in size. (d) At a critical droplet size, droplets fell down and removed from the reactor, while new droplets started to form, closing the cycle (b-d). After an initial start-up period, droplets were constantly formed and removed and the perspiration flow rate was stable. As a result, a part of the GDE surface was continuously covered with droplets, impeding the CO_2 diffusion. The spots, however, where the droplets emerged were fixed and as a result the majority of the GDE surface remained free of droplets, which explains the limited effect of perspiration on the FE of formate (Figure 8, non-saturated).

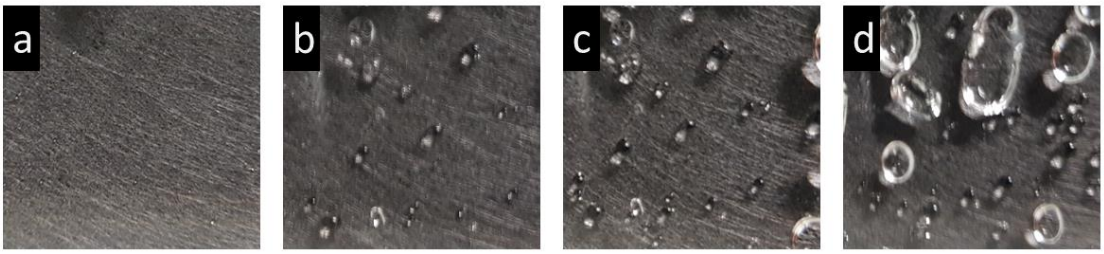

Figure 9. The four stages of perspiration: (a) dry GDE before current is applied, (b) formation of droplets once the current (100 mA/cm²) is applied, (c) the droplets grow and increase in size, (d) at a critical droplet size, the droplets are released and exit the reactor.

Next, the perspiration flow rate was measured as function of the differential pressure at both 100 mA/cm² and 0 mA/cm², the results are shown in Figure 10 and 11. Jeanty et al [26]. predicted the crystallization of electrolyte in the GDE at 0 mbar differential pressure, caused by the lack of perspiration. However, the results in Figure 10 show that this is not the case at a current density of 100 mA/cm². Due to the electro-wetting effect, minimal perspiration was observed (0.38 ml/min) at differential pressures as low as 0 mbar. This enables the use of the reactor at low differential pressures, when CO_2 diffusion is optimal, without risking crystallization of electrolyte and decreased electrode lifetime. At 0 mA/cm² it can be seen that

perspiration started only at 30 mbar differential pressure, this is ascribed to the hydrophobic character of the GDE due to the lack of electro-wetting.

In addition to the observation of the electro-wetting effect, the data from figure 10 is used to study the morphology of the GDE. At 0 mA/cm² a minimal differential pressure is required to overcome the hydrophobic character and the capillary force of the GDE and push the catholyte through the pores. This differential pressure, 30 mbar at 0 mA/cm², can be used to calculate the size of these pores using the Young-Laplace equation (Eq. 3)

$$\Delta P = \frac{2\,\gamma_{\text{water}}\,\cos\theta}{r_{\text{pore}}} \qquad \text{Eq. 3}$$

where θ is the contact angle of the water droplet and is a scale for the hydrophobicity of the GDE, γ_{water} is the surface energy of the water and r_{pore} is the radius of the pores. The physical properties of water (γ_{water} = 0.072 J/m²) and the Sigracet GDE ($\theta_{0\ mA/cm^2}$ = 150° [30]) were used to calculate the size of the pores, resulting in a 42 µm radius. Theoretically this value should be equal to the pore radius of the micro pores in the GDE surface, also called the microporous layer (MPL), which are 0.15 µm [30]. Obviously this is not the case, meaning that the radius of the micro pores in the GDE surface is not the controlling parameter during the perspiration process. This phenomenon is due to the presence of millimeter sized cracks in the surface of the blank GDE, which are visualized in Figure 12 (a) using a digital microscope (Leica M165C), an image of the spray coated GDE surface can be found in the supporting information. During the experiments, perspiration occurs at the cracks in the surface, hence the radius of the micro pores is not a controlling parameter of the process. The perspiration is controlled by the underlying structure of the GDE, also called the gas diffusion layer (GDL) which is made up of carbon fibers. The average pore radius of this underlying carbon fiber structure is 44 -42 µm [30], which is a very close approximation to the experimental value

calculated with Eq. 3. To clarify the perspiration process, it is schematically presented in Figure 12 (b).

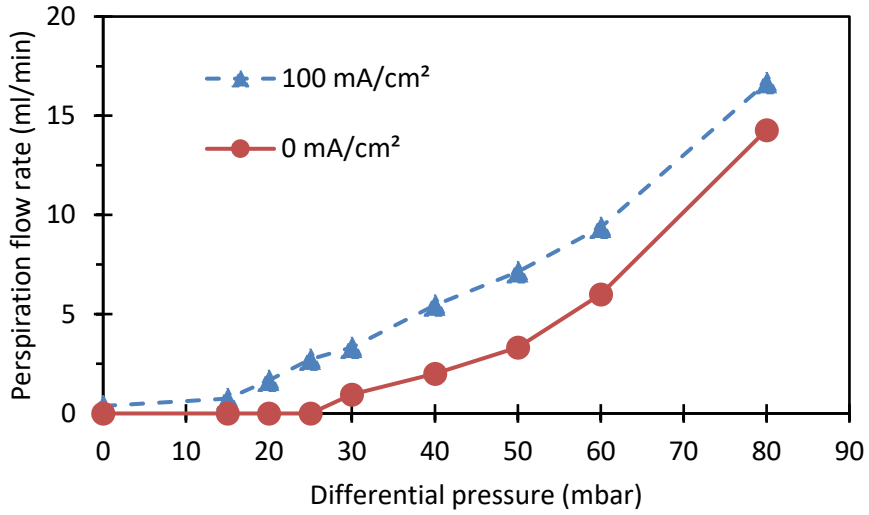

Figure 10. Influence of differential pressure on perspiration flow-rate at constant current density of 100 mA/cm² (blue, triangle) and at 0 mA/cm² (red, circle).

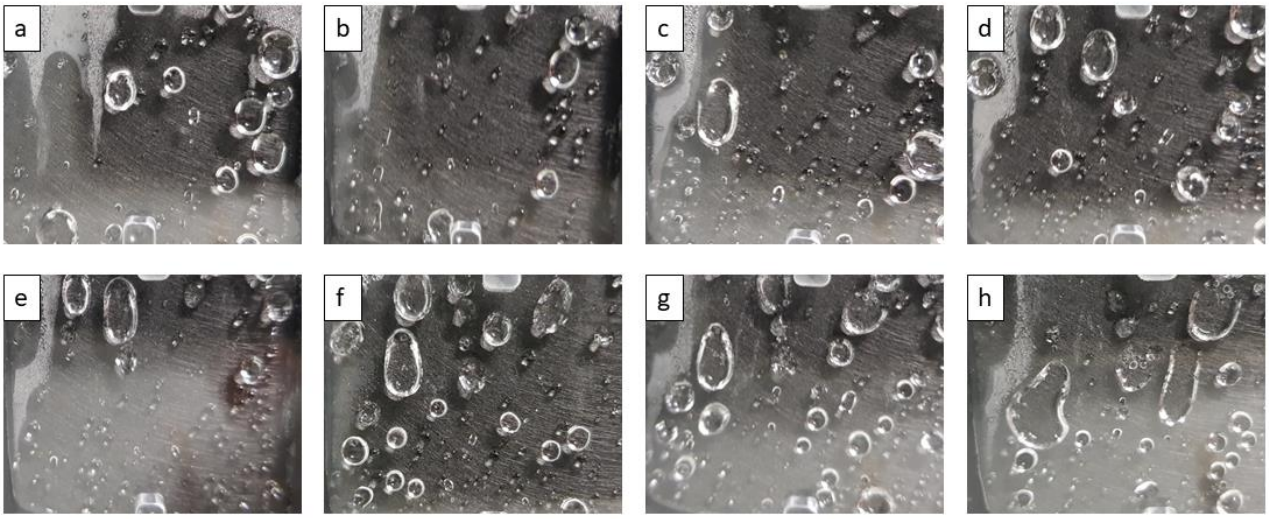

Figure 11. Flooding of perspiration at a differential pressure equal to (a) 0 mbar; (b) 10 mbar; (c) 20 mbar; (d) 30 mbar; (e) 40 mbar; (f) 50 mbar; (g) 60 mbar; (h) 80 mbar;

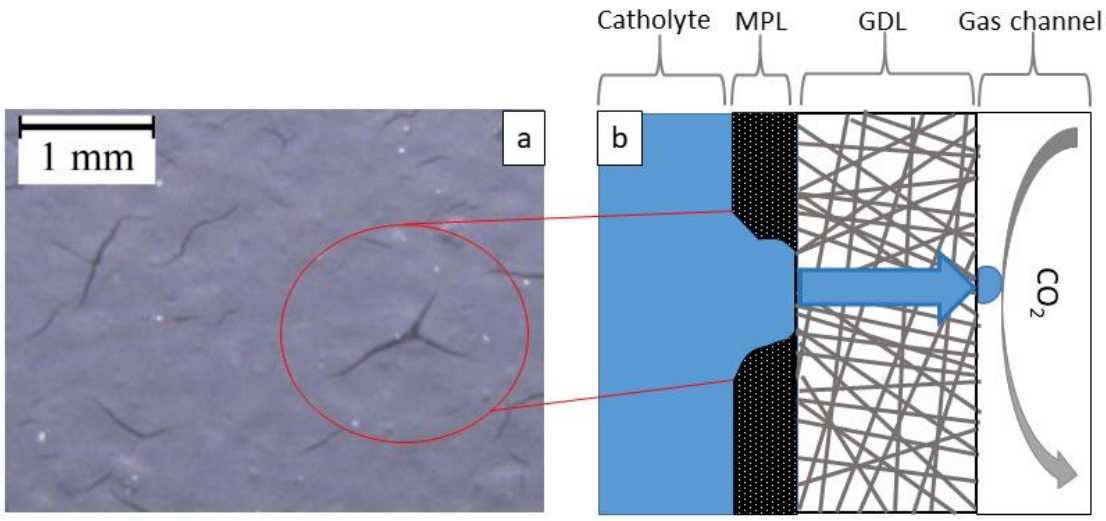

Figure 12. (a) Microscopic image of the MPL; (b) schematic presentation of the perspiration process.

These insights in the perspiration process provide an explanation for the results obtained in the previous section (§3.2). The use of non-saturated electrolyte provided a peak FE towards formate of 76% at 0 mbar differential pressure. Due to the increasing perspiration, blocking the pores of the GDE, the FE drops to 70% at 80 mbar differential pressure. Since the perspiration flow rate increased almost fifteen fold at 80 mbar compared to 0 mbar, it was expected that the influence on the FE would be much larger. As seen in Figure 12, the perspiration only took place through the cracks in the GDE surface, consequently an increase in perspiration flow rate will not lead to flooding of additional pores, but instead will result in an increased flow rate through the already flooded cracks in the surface. This is clearly shown in Figure 11 where at 0 mbar (a) 11% of the GDE surface is covered with droplets while at 80 mbar (h) only 15% of the GDE surface is covered with droplets. This minor increase of 4% in covered surface area slightly hinders the CO_2 diffusion resulting in the 6% FE decrease described in Figure 9.

From the above it is concluded that the optimal operation point for ECR in flow-by mode is at 0 mbar differential pressure due to (i) optimal CO_2 diffusion caused by minimum flooding

and (ii) sufficient flooding to prevent salt crystallization ascribed to the electro-wetting effect. In addition, due to the presence of millimeter sized cracks in the surface of the microporous layer, flooding occurs at fixed spots on the GDE surface. Therefore the rate of flooding is mainly determined by the underlying carbon fiber structure. Hence the influence of the differential pressure on the FE towards formate is 6%.

As described in the previous sections, decreasing of the differential pressure leads to a decrease in perspiration. However, at 0 mbar differential pressure, the minimum flooding is still blocking CO_2 diffusion and therefore it would be optimal if the flooding can be further minimized. Unfortunately this cannot be achieved by further lowering the differential pressure, since this will lead to negative differential pressures resulting in pushing CO_2 through the GDE and the end of flow-by operation mode. Alternatively flooding can be further minimized by changing the structure of the GDE. More specifically it is predicted that this can be achieved by altering the underlying carbon fiber structure and the PTFE content of the GDE. As shown in Eq. 3, a smaller pore radius of the carbon fiber structure will lead to a higher differential pressure needed to overcome the hydrophobicity of the pores, which will move the curves on Fig. 10 to the right. An increase of the PTFE content results in an increased hydrophobicity of the GDE and therefore a higher contact angle which will also move the curves on Figure 10 to the right. However both these changes will also have a severe influence on the three phase boundary interactions at the GDE surface and are outside the scope of this manuscript.

4. Conclusions

To raise the ECR towards an industrial scale more knowledge regarding reaction engineering has to be obtained. This work investigated the effect of the perspiration on reactor performance in a CO_2 to formate flow-by operated electrolyzer at a range of differential

pressures. The results of this investigation show that the use of non-saturated electrolyte leads to 20% FE increase due to the avoidance of a change in pH. In addition the research shows that the reactor operated at 0 mbar differential pressure provides an optimal operating point for ECR due to two major reasons: (i) minimal flooding of GDE pores resulting in increased CO_2 diffusion and (ii) sufficient perspiration to prevent the formation of salt crystals in the pores. Using these optimal parameters, a FE of 76% towards formate was achieved over a period of 6 hours at 100 mA/cm². Overall this study strengthens the idea that flow-by electrolyzers are promising reactors for the industrialization of electrochemical CO_2 conversion and pressure regulation is essential to obtain an optimal process. Additional research on the influence of the GDE structure on electrolyte flooding and FE is necessary in order to further optimize the flow-by CO_2 electrolyzer.

5. Acknowledgements

J. Hereijgers was supported through a postdoctoral fellowship (28761) of the Research Foundation – Flanders (FWO). This project was funded by the Interreg 2 Seas-Program 2014-2020, cofinanced by the European Fund for Regional Development in the frame of subsidiary contract nr. 2S03-019.

6. Conflict of interest

The authors declare no conflict of interest.

7. Bibliography

[1] R.M. Cuéllar-Franca, A. Azapagic, Carbon capture, storage and utilisation technologies: A critical analysis and comparison of their life cycle environmental

impacts, J. CO2 Util. 9 (2015) 82–102. doi:10.1016/J.JCOU.2014.12.001.

[2] O.S. Bushuyev, P. De Luna, C.T. Dinh, L. Tao, G. Saur, J. van de Lagemaat, S.O. Kelley, E.H. Sargent, What Should We Make with CO2 and How Can We Make It?, Joule. 2 (2018) 825–832. doi:10.1016/j.joule.2017.09.003.

[3] H.J. Schäfer, Contributions of organic electrosynthesis to green chemistry, Comptes Rendus Chim. 14 (2011) 745–765. doi:10.1016/j.crci.2011.01.002.

[4] J. Albo, A. Irabien, Cu2O-loaded gas diffusion electrodes for the continuous electrochemical reduction of CO2 to methanol, J. Catal. 343 (2016) 232–239. doi:10.1016/j.jcat.2015.11.014.

[5] B.C. Marepally, C. Ampelli, C. Genovese, T. Saboo, S. Perathoner, F.M. Wisser, L. Veyre, J. Canivet, E.A. Quadrelli, G. Centi, Enhanced formation of >C1 Products in Electroreduction of CO2by Adding a CO2Adsorption Component to a Gas-Diffusion Layer-Type Catalytic Electrode, ChemSusChem. 10 (2017) 4442–4446. doi:10.1002/cssc.201701506.

[6] R.A. Geioushy, M.M. Khaled, K. Alhooshani, A.S. Hakeem, A. Rinaldi, Graphene/ZnO/Cu2O electrocatalyst for selective conversion of CO2 into n-propanol, Electrochim. Acta. 245 (2017) 456–462. doi:10.1016/j.electacta.2017.05.185.

[7] J. Shi, Q.-Y. Li, F. Shi, N. Song, Y.-J. Jia, Y.-Q. Hu, F. Shen, D. Yang, Y.-N. Dai, Design of a Two-Compartment Electrolysis Cell for the Reduction of CO_2 to CO in Tetrabutylammonium Perchlorate/Propylene Carbonate for Renewable Electrical Energy Storage, J. Electrochem. Soc. 163 (2016) G82–G87. doi:10.1149/2.1381607jes.

[8] Q. Wang, H. Dong, H. Yu, H. Yu, M. Liu, Enhanced electrochemical reduction of carbon dioxide to formic acid using a two-layer gas diffusion electrode in a microbial electrolysis cell, RSC Adv. 5 (2015) 10346–10351. doi:10.1039/C4RA14535F.

[9] R.L. Machunda, J. Lee, J. Lee, Microstructural surface changes of electrodeposited Pb

on gas diffusion electrode during electroreduction of gas-phase CO2, Surf. Interface Anal. 42 (2010) 564–567. doi:10.1002/sia.3245.

[10] O.G. Sánchez, Y.Y. Birdja, M. Bulut, J. Vaes, T. Breugelmans, D. Pant, Recent advances in industrial CO2 electroreduction, Curr. Opin. Green Sustain. Chem. (2019). doi:10.1016/J.COGSC.2019.01.005.

[11] M. Le, M. Ren, Z. Zhang, P.T. Sprunger, R.L. Kurtz, J.C. Flake, Electrochemical Reduction of CO2 to CH3OH at Copper Oxide Surfaces, J. Electrochem. Soc. 158 (2011) E45. doi:10.1149/1.3561636.

[12] C. Dinh, T. Burdyny, G. Kibria, A. Seifitokaldani, C.M. Gabardo, F.P.G. de Arquer, A. Kiani, J.P. Edwards, P. De Luna, O.S. Bushuyev, C. Zou, R. Quintero-Bermudez, Y. Pang, D. Sinton, E.H. Sargent, Sustained high-selectivity CO 2 electroreduction to ethylene via hydroxide-mediated catalysis at an abrupt reaction interface. Submitted to, Science (80-.). 787 (2018) 783–787. doi:10.1126/science.aas9100.

[13] A. Engelbrecht, M. Hämmerle, R. Moos, M. Fleischer, G. Schmid, Improvement of the selectivity of the electrochemical conversion of CO2 to hydrocarbons using cupreous electrodes with in-situ oxidation by oxygen, Electrochim. Acta. 224 (2017) 642–648. doi:10.1016/j.electacta.2016.12.059.

[14] H.-R. “Molly” Jhong, F.R. Brushett, P.J.A. Kenis, The Effects of Catalyst Layer Deposition Methodology on Electrode Performance, Adv. Energy Mater. 3 (2013) 589–599. doi:10.1002/aenm.201200759.

[15] C. Zhao, J. Wang, J.B. Goodenough, Comparison of electrocatalytic reduction of CO2to HCOOH with different tin oxides on carbon nanotubes, Electrochem. Commun. 65 (2016) 9–13. doi:10.1016/j.elecom.2016.01.019.

[16] K. Weissermel, H.-J. Arpe, Wiley InterScience (Online service), Industrial organic chemistry, Wiley-VCH, 2003.

[17] D.T. Whipple, E.C. Finke, P.J.A. Kenis, Microfluidic Reactor for the Electrochemical Reduction of Carbon Dioxide: The Effect of pH, Electrochem. Solid-State Lett. 13 (2010) B109. doi:10.1149/1.3456590.

[18] I. Merino-Garcia, E. Alvarez-Guerra, J. Albo, A. Irabien, Electrochemical membrane reactors for the utilisation of carbon dioxide, Chem. Eng. J. 305 (2016) 104–120. doi:10.1016/j.cej.2016.05.032.

[19] J.-B. Vennekoetter, R. Sengpiel, M. Wessling, Beyond the catalyst: How electrode and reactor design determine the product spectrum during electrochemical CO2 reduction, Chem. Eng. J. 364 (2019) 89–101. doi:10.1016/J.CEJ.2019.01.045.

[20] B. Endrődi, G. Bencsik, F. Darvas, R. Jones, K. Rajeshwar, C. Janáky, Continuous-flow electroreduction of carbon dioxide, Prog. Energy Combust. Sci. 62 (2017) 133–154. doi:10.1016/J.PECS.2017.05.005.

[21] S. Pérez-Rodríguez, F. Barreras, E. Pastor, M.J. Lázaro, Electrochemical reactors for CO2reduction: From acid media to gas phase, Int. J. Hydrogen Energy. 41 (2016) 19756–19765. doi:10.1016/j.ijhydene.2016.06.130.

[22] D.A. Vermaas, W.A. Smith, Synergistic Electrochemical CO2 Reduction and Water Oxidation with a Bipolar Membrane, ACS Energy Lett. 1 (2016) 1143–1148. doi:10.1021/acsenergylett.6b00557.

[23] H.-R. “Molly” Jhong, S. Ma, P.J. Kenis, Electrochemical conversion of CO2 to useful chemicals: current status, remaining challenges, and future opportunities, Curr. Opin. Chem. Eng. 2 (2013) 191–199. doi:10.1016/J.COCHE.2013.03.005.

[24] K. Liu, W.A. Smith, T. Burdyny, Introductory Guide to Assembling and Operating Gas Diffusion Electrodes for Electrochemical CO_2 Reduction, ACS Energy Lett. 4 (2019) 639–643. doi:10.1021/acsenergylett.9b00137.

[25] S. Ma, M. Sadakiyo, R. Luo, M. Heima, M. Yamauchi, P.J.A. Kenis, One-step

electrosynthesis of ethylene and ethanol from CO2 in an alkaline electrolyzer, J. Power Sources. 301 (2016) 219–228. doi:10.1016/J.JPOWSOUR.2015.09.124.

[26] P. Jeanty, C. Scherer, E. Magori, K. Wiesner-Fleischer, O. Hinrichsen, M. Fleischer, Upscaling and continuous operation of electrochemical CO2 to CO conversion in aqueous solutions on silver gas diffusion electrodes, J. CO2 Util. 24 (2018) 454–462. doi:10.1016/J.JCOU.2018.01.011.

[27] A. Del Castillo, M. Alvarez-Guerra, J. Solla-Gullón, A. Sáez, V. Montiel, A. Irabien, Electrocatalytic reduction of CO2to formate using particulate Sn electrodes: Effect of metal loading and particle size, Appl. Energy. 157 (2015) 165–173. doi:10.1016/j.apenergy.2015.08.012.

[28] I. Merino-Garcia, J. Albo, A. Irabien, Tailoring gas-phase CO_2 electroreduction selectivity to hydrocarbons at Cu nanoparticles, Nanotechnology. 29 (2018) 014001. doi:10.1088/1361-6528/aa994e.

[29] S. Verma, X. Lu, S. Ma, R.I. Masel, P.J.A. Kenis, The effect of electrolyte composition on the electroreduction of CO_2 to CO on Ag based gas diffusion electrodes, Phys. Chem. Chem. Phys. 18 (2016) 7075–7084. doi:10.1039/C5CP05665A.

[30] R. Schweiss, R. Schweiss, C. Meiser, T. Damjanovic, I. Galbiati, N. Haak, SIGRACET® Gas Diffusion Layers for PEM Fuel Cells, Electrolyzers and Batteries (White Paper) View project Vanadium redox flow battery View project SIGRACET® Gas Diffusion Layers for PEM Fuel Cells, Electrolyzers and Batteries, n.d. www.sigracet.com (accessed January 23, 2019).